A theoretical and experimental approach to shell-isolated nanoparticle-enhanced Raman spectroscopy of single-crystal electrodes

ARTICLE *in* SURFACE SCIENCE · JANUARY 2015

Impact Factor: 1.93 · DOI: 10.1016/j.susc.2014.07.019

4 AUTHORS, INCLUDING:

Song-Yuan Ding
Xiamen University
15 PUBLICATIONS **201** CITATIONS
SEE PROFILE

Jun Yi
Xiamen University
3 PUBLICATIONS **13** CITATIONS
SEE PROFILE

Zhong-Qun Tian
Xiamen University
354 PUBLICATIONS **9,823** CITATIONS
SEE PROFILE

Surface Science 631 (2015) 73–80

Contents lists available at ScienceDirect

Surface Science

journal homepage: www.elsevier.com/locate/susc

A theoretical and experimental approach to shell-isolated nanoparticle-enhanced Raman spectroscopy of single-crystal electrodes

Song-Yuan Ding [a,*], Jun Yi [b], Jian-Feng Li [c], Zhong-Qun Tian [a,b,**]

[a] Collaborative Innovation Center of Chemistry for Energy Materials (iChEM), Xiamen University, Xiamen 361005, China
[b] State Key Laboratory of Physical Chemistry of Solid Surfaces and College of Chemistry and Chemical Engineering, Xiamen University, Xiamen 361005, China
[c] MOE Key Laboratory of Analytical Sciences, Xiamen University, Xiamen 361005, China

ARTICLE INFO

Available online 23 July 2014

Keywords:
Surface-enhanced Raman spectroscopy
Surface plasmon resonance
SHINERS
Single-crystal electrodes

ABSTRACT

Recently we developed shell-isolated nanoparticle-enhanced Raman spectroscopy (SHINERS) as a new variant of surface-enhanced Raman spectroscopy (SERS). The most important feature of SHINERS is its capability to study electrochemical single-crystal electrode surfaces, e.g., gold, platinum, palladium, rhodium and silicon. The gold-core silica-shell nanoparticles can significantly boost the Raman intensity from adsorbates on atomically flat surfaces. Very surprisingly the average enhancement factor can reach 10^6 for Au(110) and 10^5 for Pt(110). To understand this extraordinary high enhancement, we explore the mechanism on why SHINERS works so well for single-crystal electrode of diverse materials by classical electromagnetic simulations. We then performed the periodic DFT calculations of the polarizability of clean and pyridine-modified surfaces and the Raman intensity of adsorbates to reveal the interesting phenomenon regarding surface-crystal-orientation dependence of SHINERS intensity. Finally, prospective developments of EC-SHINERS are discussed.

1. Introduction

Interfacial electrochemistry, especially adsorption and electrocatalysis at single-crystal electrodes in contact with electrolyte solutions is of great importance in fundamental researches on energy conversion, material transformation, environment protection, industrial processes, etc. [1,2] The in situ spectroelectrochemical (SEC) characterization of atomic and electronic structures of single-crystal electrodes/electrolyte interfaces and their dynamics would help us to well understand the electrode processes at both of macroscopic and microscopic levels [3]. Raman spectroscopy can provide vibrational fingerprint spectra and exclude the interference of water molecules in typical electrochemical systems. Because of the intriguing features, Raman spectroscopy was considered as an ideal in situ SEC technique to detect the surface bonding between adsorbates and the electrodes, determine the adsorption sites and molecular configuration and even monitor electrochemical reactions [4,5]. However, conventional Raman scattering is intrinsically very weak and cannot be used for surface characterization. Raman signal can be significantly enhanced by virtue of the surface-enhance Raman scattering (SERS) effect [6–10]. This is primarily a phenomenon associated with the amplification of Raman signals of analytes adsorbed on or very close to the nanostructures with free-electron metal (i.e., gold, silver and copper) and dielectric interfaces by several orders of magnitude due to the enhanced local electromagnetic (EM) fields and the enhanced scattering efficiency generated by surface-plasmon resonance (SPR) [11,12].

In SERS, only analytes sit on or very close to the SERS-active substrates have the SERS effect. If SERS enhancement factor (EF) is 10^6, the Raman signals from monolayer species on electrodes are comparable to 10^5–10^6 layer molecules without any enhancement. Therefore, SERS is indeed one of the intrinsic surface-sensitive tools (SERS, vibrational sum-frequency generation, surface-enhanced infrared spectroscopy, STM, etc.) for which interfaces make preeminent contribution to the measured signals [3].

However, only a few free-electron metal materials, mainly Ag, Au, and Cu, have a giant SERS effect, which severely limits the breadth of practical applications of SERS in other materials, e.g., Pt, Fe, Ni, and semiconductors, widely used in corrosion, electrocatalysis and other electrochemical industries. In addition, the roughness of the metal surface and the patterned surfaces, or the colloid size of SERS substrates must be at the scale of several tens of nanometers, which confines SERS studies to surfaces or interfaces with ill-defined morphology that are not of common interests in the community of surface science [13]. These two limitations stem from the plasmonic nature of SERS substrates and from the fact that the traditional SERS-active electrodes typically have dual functions, the SERS enhancer and molecular supporter.

Although tip-enhanced Raman spectroscopy (TERS) [14] and attenuated total reflection (ATR) [15,16] can also increase the Raman

* Corresponding author.
** Correspondence to: Z.-Q. Tian, Collaborative Innovation Center of Chemistry for Energy Materials (iChEM), Xiamen University, Xiamen 361005, China.
E-mail addresses: xmu.syding@gmail.com (S.-Y. Ding), zqtian@xmu.edu.cn (Z.-Q. Tian).

http://dx.doi.org/10.1016/j.susc.2014.07.019
0039-6028/

signal strength in the study of single crystal surfaces, these two methods have their own limitations. The average EF of ATR-mode Raman is only 1 to 2 orders of magnitude although the number of molecules sampled is large. The average EFs of TERS can reach up to 5 orders of magnitude, but few molecules underneath the tip can be sampled. Therefore, it is still necessary to develop new structurally sensitive in situ SEC techniques.

Recently we developed a new member of the SERS family, shell-isolated nanoparticle-enhanced Raman spectroscopy (SHINERS) [17]. In SHINERS, the Raman signal amplification is provided by Au or Ag nanoparticles (NPs) with an ultrathin silica or alumina shell (Fig. 1). A monolayer of such shell-isolated NPs (SHINPs) is spread as 'smart dust' over the surface that is to be probed. The ultrathin isolating shell, which is made of a chemically inert dielectric shell that prevents direct contact between the core and the species under study thereby mitigates the risk of interference, and at the same time supports the long-range EM field provided by the plasmonic Au/Ag core. SHINERS of pyridine on Au(*hkl*), and Pt(*hkl*) surfaces [18,19], SCN^-/2,2′-bipyridine on Au(hkl) [17,20], hydrogen on Pt(111) and Rh(111) [17,21], benzotriazole on Cu(*hkl*) [22] and even hydrogen on Si have been reported. However, we have not very clearly understood the working principle of SHINERS on single-crystal surfaces.

In the following section, we first briefly introduce the experimental procedures of a typical electrochemical SHINERS (EC-SHINERS) measurement, then we focus on the working principle of SHINERS and facet-dependent SHINERS effect on the single-crystal surfaces in electrochemical systems. Finally, we will give the prospective on the emerging methodologies in view of new EC-SHINERS substrates, methods and techniques for in situ electrochemical studies.

2. Electrochemical shell-isolated nanoparticle-enhanced Raman spectroscopy

2.1. Preparation of shell-isolated nanoparticles and EC-SHINERS measurements

The SHINPs consist of NPs with noble-metal core and ultrathin chemical-inert overlayer. As shown in Fig. 1, the core material can be gold [17] or silver [23], the size of the core spheres can be 55 nm or much larger up to 120 nm [24] for different working conditions, the shape of core can be sphere, cube [25] or rod [26] for different working wavelength of incident light, the shell materials can be SiO_2, Al_2O_3 [17,27], MnO_2 [28] and Ag_2S [29] working in different pH conditions. Typically, the shell thickness should be less than 3 nm and pin-hole free.

A schematic of a typical EC-SHINERS experiment was illustrated in Fig. 2. When the SHINPs were successfully synthesized [27] and

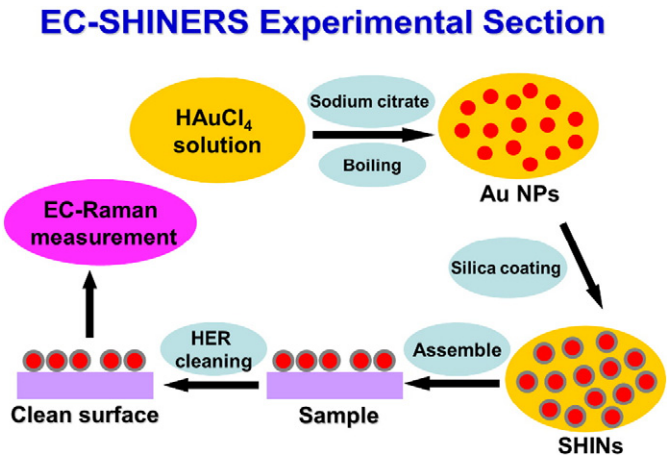

Fig. 2. Schematic illustration of the electrochemical SHINERS experiment.

self-assembled on the electrodes, the pretreatment of the SHINPs-modified (single-crystal) electrodes with hydrogen evolution reduction (HER) method is very necessary for the weak-adsorbed systems under study [19]. That is because the SHINPs may block the surface sites or release organic contaminants from the NPs preparation, and further influence the double layer and the oxidation/reduction response of electrolytes severely.

An Au(*hkl*) electrode modified with SHINPs was mounted in a three-electrode thin-layer cell in a vertical configuration filled with deoxygenated neutral 0.1 M $NaClO_4$ solution. Next, the electrode was polarized at −2.0 V (vs. Ag/AgCl) for 50 to 100 s. The HER proceeds vigorously. However, the thin layer geometry prevents the formation of big hydrogen bubbles, which keeps the submonolayer of NPs rather stable. The impurities desorbed from the surface at so negative potential and diffused to the solution. Then this polarization procedure was repeated 3 to 4 times, accompanied by cycles of solution exchange to remove the desorbed impurities.

The voltammetric experiments of the HER-treated Au(111) electrode were performed in 0.1 M H_2SO_4 or 0.1 M $HClO_4$ (blue solid lines in Fig. 3). The lifting/reformation of the surface reconstruction (P_1/P_1'), the disorder/order phase transition within the sulfate adlayer (P_3/P_3'), as well as surface oxidation (P_4, P_5) and reduction (P_5'), show almost identical response as the ideally smooth Au(111) NP-free surface (black lines in Fig. 3), while the dotted curves are obtained in the presence of "as-prepared" SHINPs [19].

With the help of SHINPs, we can obtain several high-quality surface Raman spectra from adsorbates on single crystal surfaces with varies

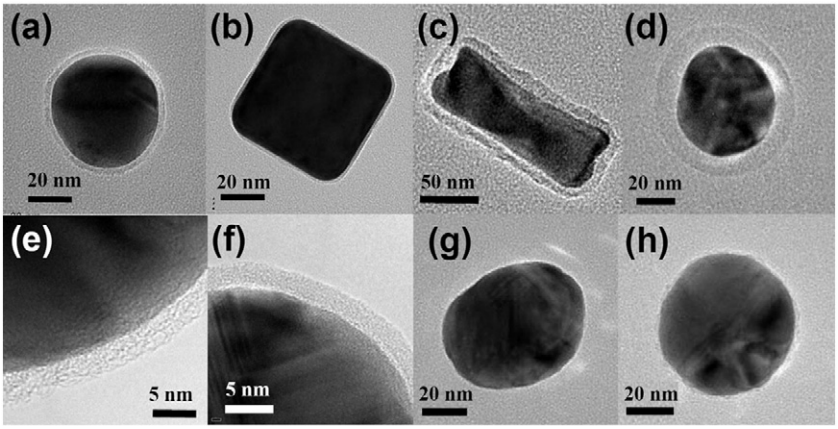

Fig. 1. TEM images of various kinds of SHINPs. (a) 55 nm Au@SiO_2 (b) cube and (c) rod Au@SiO_2 and (d) Ag@SiO_2 SHINPs, and the Au nano-sphere can be coated with different materials: (e) SiO_2, (f) Al_2O_3, (g) MnO_2 and (h) Ag_2S.

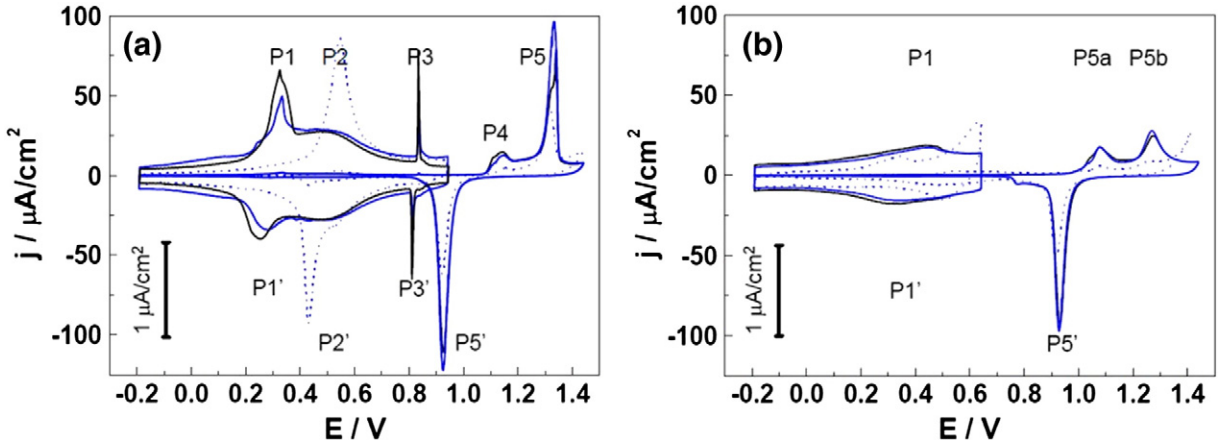

Fig. 3. CVs of Au(111)-(1 × 1) single-crystal bead electrodes unmodified (black lines) and modified (solid blue lines) with Au@SiO_2 SHINPs. The dotted blue traces were recorded with unpretreated SHINPs, while the solid blue lines represent data obtained with HER pretreated SHINPs. The voltammograms in the double layer region are displayed with a magnification factor of 30. Solution: 0.1 M (a) H_2SO4 and (b) $HClO_4$. Scan rate: 10 mV/s.
Reproduced by permission of American Chemical Society, from Li et al. [19].

materials in electrochemical systems. As shown in Fig. 4a, the average enhancement factors (EFs) of SHINERS spectra of pyridine on Au(110) is about 10^6. This result is quite surprising because for incident polarization along the center axis of two spherical particles, EM coupling between gold NPs has long been considered to be much stronger than that between NPs and smooth surfaces. More interesting, we found that if the size parameter of the SHINPs and the excitation wavelength 632.8 nm are fixed, we can always get high-quality SHINER spectra on many different metallic single-crystal surfaces other than gold and silver, such as platinum (Fig. 4b), palladium, rhodium and even silicon. These surprising phenomena motivate us to study the physical mechanism behind.

2.2. Theoretical study on SHINERS of single-crystal electrodes

The finite element method based package COMSOL 4.3b, was employed as an EM solver to simulate the extinction spectra and the local EM field in the vicinity of SHINPs-surface systems. We used the dielectric constants of gold, copper, nickel and palladium from Johnson & Christy's experimental data, and interposed more points from 500 to 700 nm with cubic spline method. The refractive index of silica is kept 1.55 from 350 to 900 nm. The Au@SiO_2 NP is 55 nm in core size and 2 nm in shell thickness. The spacing between the neighboring Au@SiO_2 is 2 nm, and Au@SiO_2 is directly contacted with the single crystal surfaces (Fig. 5).

As shown in Fig. 6a, there is a dip around 600 nm and two peaks at 555 and 655 nm in the extinction spectrum. If the incident and scattered wavelengths are very close, the EF of SERS can be approximated as the fourth power of the EF of EM field [30]. Fig. 7a, b and c shows the simulated distribution of $\log_{10}|\mathbf{E}|^4$ at the very wavelengths (555, 600, 655 nm) of the incident light for two Au@SiO_2 NPs on flat Au surfaces. It is noted that the EM field is highly localized at two points. One is the contact point between Au@SiO_2 NPs and Au surface (denoted as point A), and the other one locates at the gap between NPs (denoted as point B). Therefore, points A and B can be regarded as SERS hot spots, i.e. molecules adsorbed at the site around the two points will contribute to most of the SERS signals.

In order to obtain the SHINER spectra on single-crystal surfaces with much higher EFs, and in order to clearly understand the behaviors of localized hot spots at A and B, we further plotted the norm of electric field of at point A and B with respect to the excitation wavelength. As shown in Fig. 6b, the changing trend of EM fields of points A and B can be

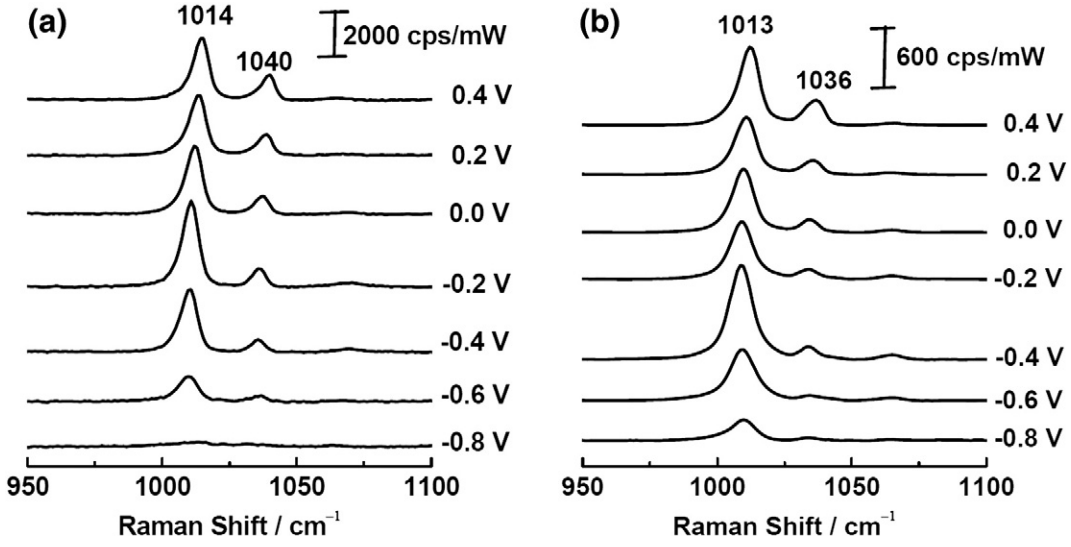

Fig. 4. (a) SHINER spectra of pyridine on Au(110) and (b) that on Pt(110) at different potentials. Electrolyte: 10 mM pyridine + 0.1 M $NaClO_4$.

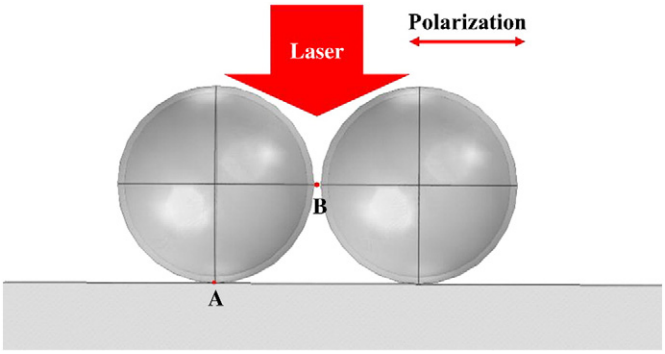

Fig. 5. The finite element method (FEM) simulation model of a 2 × 1 array of 55 nm Au@2 nm SiO_2 NPs placed on a single-crystal surface which can be made of gold, silver, copper, nickel, silicon, etc. The shell to shell distance is 2 nm. The polarization of the incident light is parallel to the surface.

divided into four stages. As the excitation wavelength ranging from 500 nm to 555 nm, the EM field strength at both points A and B increases and the EM field between the two SHINPs (point B) is slightly higher. In the second stage (excitation wavelength of 555 to 600 nm), the EM field strength decreases at point B but still increases at point A.

Furthermore, it is noted that the EM field at point A becomes higher. In other words, there is a "hot-spot transfer" phenomenon from the gap between NPs to the contact point between NPs and substrates for Au@SiO_2-Au(*hkl*) systems [18,31]. In the third stage, both the strengths of EM field at points A and B increase with the excitation wavelength and reach a maximum at ~655 nm. Finally, the EM field strength falls down with the further increase of excitation wavelength (see also Fig. 7d). Based on above results, in order to obtain the maximum SERS enhancement (EM enhancement at both incidents and Raman scattering frequency), we'd better choose excitation wavelength in this regime, from 620 to 650 nm. Practically, we used a 632.8 nm laser as the excitation line. The detailed plasmonic mode analysis of the Au@SiO_2–Au(*hkl*) systems will be published elsewhere [31].

More interestingly, Au@SiO_2 SHINPs on different metal surfaces (Au, Ag, Au, Pt, Pd, Ni, Rh, etc.) show very similar plasmonic profiles both in extinction and near field. The apparent difference is the absolute EM intensities of the near field. Our results show that the near field in Au@SiO_2 on coinage substrates systems is typically larger than that for Au@SiO_2 on TM surfaces (Fig. 8). Therefore, SHINERS in principle works well on both of coinage and TM single-crystal surfaces.

In the case of Au@SiO_2 NPs on flat dielectric surfaces, see Fig. 9, although there is no hot-spot transfer effect in Au@SiO_2-Si-surface system, the near field at points A and B indeed can reach the maxima at ~600 nm. Therefore, in principle we still can obtain the Raman signals of adsorbates on atomic flat Si surfaces, although the species in the gap of Au@SiO_2 may also contribute to overall Raman spectra. Actually, we indeed have obtained a SHINER spectrum of Si – H stretching mode on Si(111) wafer treated with 30% HF solution [17]. Our preliminary simulation shows that the maximum enhancement factor will decrease as the dielectric constants of the substrates decrease if the illumination configuration is kept normal. However, we can win additional SHINERS enhancement from the side illumination setup. In this case, we should modify the laser incident angle to the probed surface in practice.

In addition, our experiments show that the absolute SHINERS intensities strongly depend on the surface crystal orientation of the same metal surfaces [18]. As shown in Fig. 10a, the SHINER intensity of the ring breathing normal mode of pyridine on Au(110) is about eight times stronger than that on Au(100) and about 30 times stronger than that on Au(111) at a substrate potential of 0.00 V. Fig. 10b further illustrates that this trend is independent of the applied potential. It should be noted that, the enhancement factor of SHINERS on Pt surfaces follows the same order, Pt(110) > Pt(100) > Pt(111) [18].

In order to better understand this facet-dependent Raman effect, we performed the periodic DFT calculations of the polarizability of clean surfaces and overlayered surfaces, and the Raman intensity of adsorbed molecules using Vienna ab initio simulation package (VASP) [32] with PBE functional for exchange-correlation energy. The projector augmented wave (PAW) method was employed to account for electron–ion interactions. The plane wave kinetic energy cutoff was set to 400 eV throughout all calculations. A 9 × 9 × 1 Monkhorst–Pack grid of k-points was applied in the self-consistent field calculations. The molecule-surface system was modeled by a repeated slab consisting of five atomic layers thick and separated by a vacuum layer of 25 Å. The adsorption configurations of a pyridine molecule on Au(111), Au(100) and Au(110) on the atop site via nitrogen atom was all modeled by a (2 × 2) supercell structures (Fig. 11) which is a good approximation to the realistic systems at the voltage close to 0.0 V except for Au(110) [33]. When performing the geometry optimizations, all atoms of pyridine and the upmost two gold layers were relaxed until the largest remaining Hellmann–Feynman force was smaller than 0.01 eV $Å^{-1}$. The bottom three gold layers were kept fixed with the optimized bulk lattice constant of $a_{fcc} = 4.174$ Å.

Due to the surface selection rule of SERS, the SERS signal is dominated by the *zz* component of the polarizability derivatives (α'_{zz}). Thus we only calculated the *zz* component of polarizability derivatives, and the Raman scattering factor was be approximated as $S_k \sim 12(\partial\alpha_{zz}/\partial Q_k)^2$.

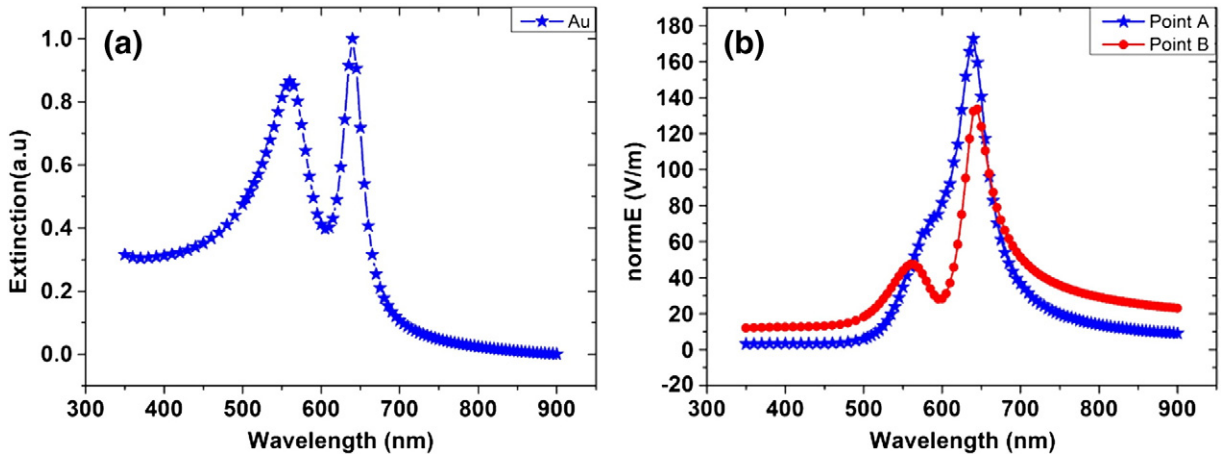

Fig. 6. The simulated normalized extinction (a) and the norm of electric field of Au@SiO_2 on flat Au surfaces (b). Here, points A and B are the two representative points between two SHINPs, and between SHINP and substrates, respectively. The illumination configuration is depicted in Fig. 5.

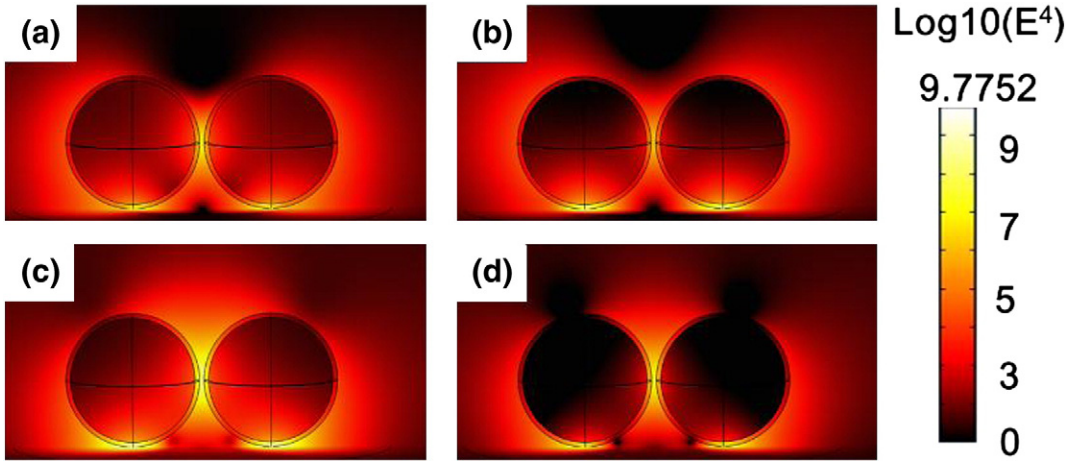

Fig. 7. The simulated distribution of $\log_{10}|\mathbf{E}|^4$ as a function of the wavelength of incident light (a) 555 nm (the first peak in the extinction spectrum of Fig. 6a), (b) 600 nm (the dip in the extinction spectrum of Fig. 6a), (c) 655 nm (the second peak in the extinction spectrum of Fig. 6a) and (d) 700 nm.

Here both of α_{zz} and its derivative $\partial\alpha_{zz}/\partial Q_k$ were calculated with numerical difference methods. We have also tested the numerical stability of the polarizability with a series of the differential step size of perturbing electrostatic field strengths from 0.001 to 0.4 V/Å, and found that a stable polarizability cannot be obtained with field strength less than 0.04 V/Å. Therefore, we used an external field strength of 0.1 V/Å in practice. The displacement was scaled to half of the normalized mass-weighted normal modes [18]. It should be noted that, the present computation cost of a surface Raman spectrum is extremely expensive, since the self-consistent-field calculation of metals under external electrostatic field is very hard to converge. Because of the limited computation source, we only calculate the ring breathing mode υ_1 which is the mode with the strongest Raman intensity in pyridine.

Table 1 shows that the interaction between pyridine and a gold surfaces increases in the order Au(111) < Au(100) < Au(110). This sequence is consistent with the experimental data for slightly positively charged interfaces on which pyridine is coordinated to each Au(*hkl*) through the lone pair electrons of the nitrogen heteroatom of pyridine. For the negatively charged interfaces, pyridine will be coordinated to Au(111) through π-bond, then the adsorption energy of pyridine-Au(111) may be larger than pyridine-Au(110) or Au(100) [42,43]. It is interesting that both the clean surface and the pyridine-modified surface become increasingly polarizable in the *z* direction following the same order, and the Raman intensity of the υ_1 mode also gets stronger from Au(111) to Au(110). Our first principle simulation of the pyridine-Au surfaces well reproduces the trends but not the magnitude of the Raman intensities of the υ_1 mode. However, our calculation indeed reveals that the polarizability of the unit cell or optical dielectric constant of different crystal orientation may be slightly different. If we further consider the strong plasmonic/EM coupling between Au@SiO_2 SHINPs and Au(hkl), this small difference in dielectric constants may result in a large difference in the enhancement factors of SHINER spectra.

Since bare Au NPs in solutions suffer from aggregation, the aging problem leads to the reproducibility problems in practical applications. In contrast, shell-isolated NPs in solution are very stable, and can maintain a reproducible enhanced Raman signal for five days. In addition, the isolated and chemical inert shell in SHINPs can prevent hot-carrier transfer from SHINPs to molecules which may make the in situ characterizations of plasmon-mediated photocatalytic or photo-electrocatalytic reactions more reliable [34]. All of the aforementioned novel features make SHINERS as a general and reliable analytic tool for in situ electrochemical studies of electro-adsorption and electrocatalysis of redox or photocatalyzed redox processes.

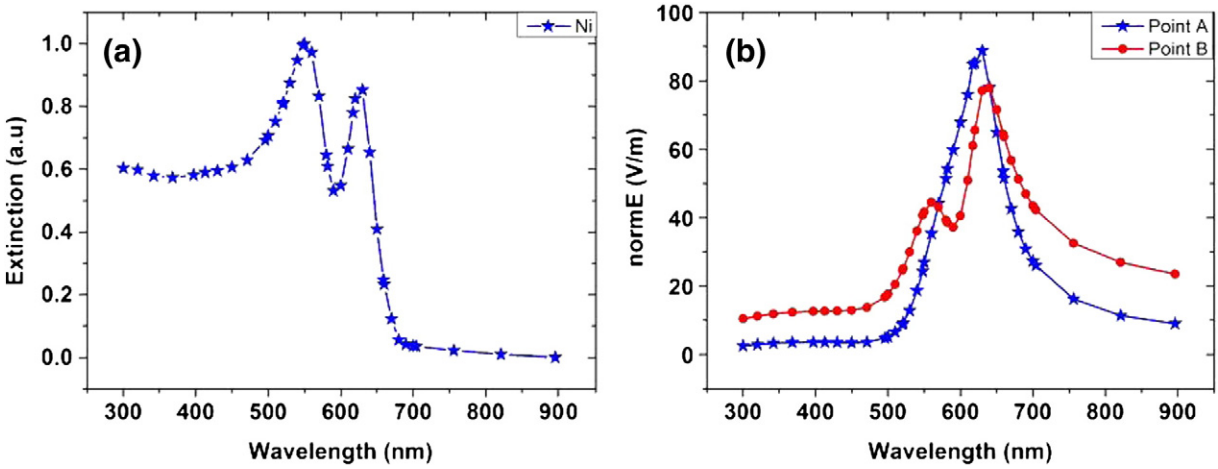

Fig. 8. The simulated normalized extinction (A) and the norm of electric field of Au@SiO_2 on flat Ni surfaces. The illumination configuration is depicted in Fig. 5.

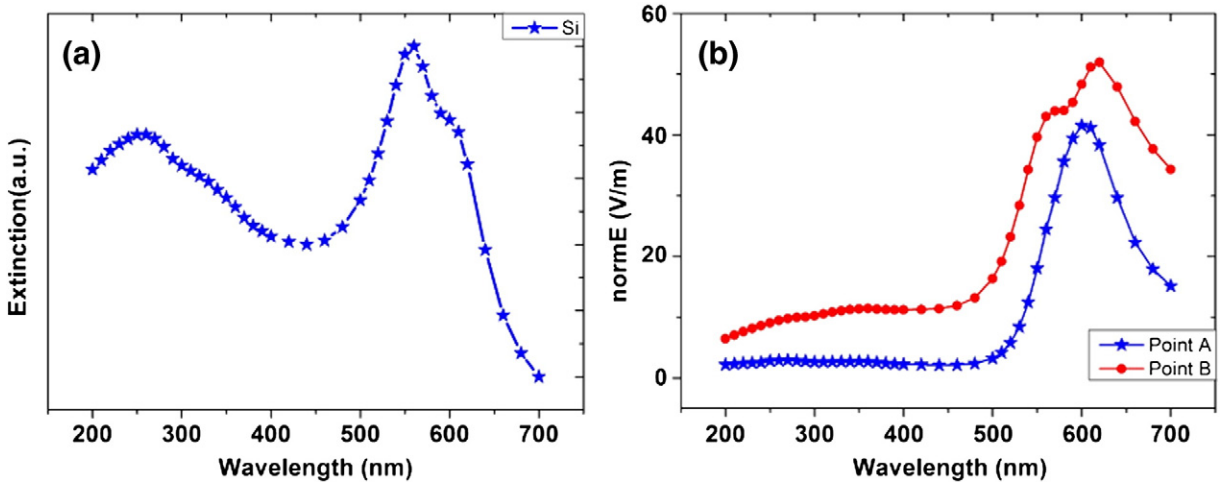

Fig. 9. The simulated normalized extinction (A) and the norm of electric field of Au@SiO_2 on flat Si surfaces. The illumination configuration is depicted in Fig. 5.

3. Conclusions and outlook

It has been shown that SHINERS is a powerful and intrinsic surface-science analytic tool with impressive generality and high reliability. Especially, SHINERS can in principle be applied to in situ electrochemical studies on single-crystal electrode surfaces of diverse materials, including all of the solid metals and most of the semiconductors and insulators. The following several approaches could further improve the sensitivity, resolution, generality and reliability of SHINERS in the near future.

It is interesting and meaningful to theoretically study the EM coupling between SHINPs and the more complex nanostructured electrodes, which is unavoidable in practical application of SHINERS. Furthermore, new shell-isolated plasmonic nanostructures supporting Fano-resonance [35,36] or double resonance [37,38], directional antenna [39], high-density SERS hot spots [40], etc. will be very useful to improve the detection sensitivity of SHINERS due to further increase of the maximal local EM field and largest transition efficiency of the scattered field.

Moreover, the shell-isolated strategy could in principle be extended to other active substrates for surface-enhanced spectroscopies, such as shell-isolated tip-enhanced Raman spectroscopy (SHI-TERS), shell-isolated nanoparticle-enhanced fluorescence (SHINEF) [41], shell-isolated nanoparticle-enhanced infrared spectroscopy (SHINE-IRS), shell-isolated nanoparticle-enhanced sum frequency generation (SHINE-SFG) and shell-isolated nanoparticle-enhanced CARS (SHINE-CARS). The shell-isolated TERS and shell-isolated nanoparticle-enhanced spectroscopies can then avoid the signal interference from the adsorbates directly contact with SES-active nanostructures. SHINEF can further intrinsically avoid the fluorescence quenching effect. More importantly, the shell-isolated strategy can effectively improve the stability of the active substrates under ultrafast illumination especially for some surface-enhanced nonlinear spectroscopies and time-resolved surface-enhanced spectroscopies.

The re-combination of single-crystal electrochemistry and surface spectroscopy, and characterization and theoretical methods would help us to realize the chemical imaging of electrochemical processes,

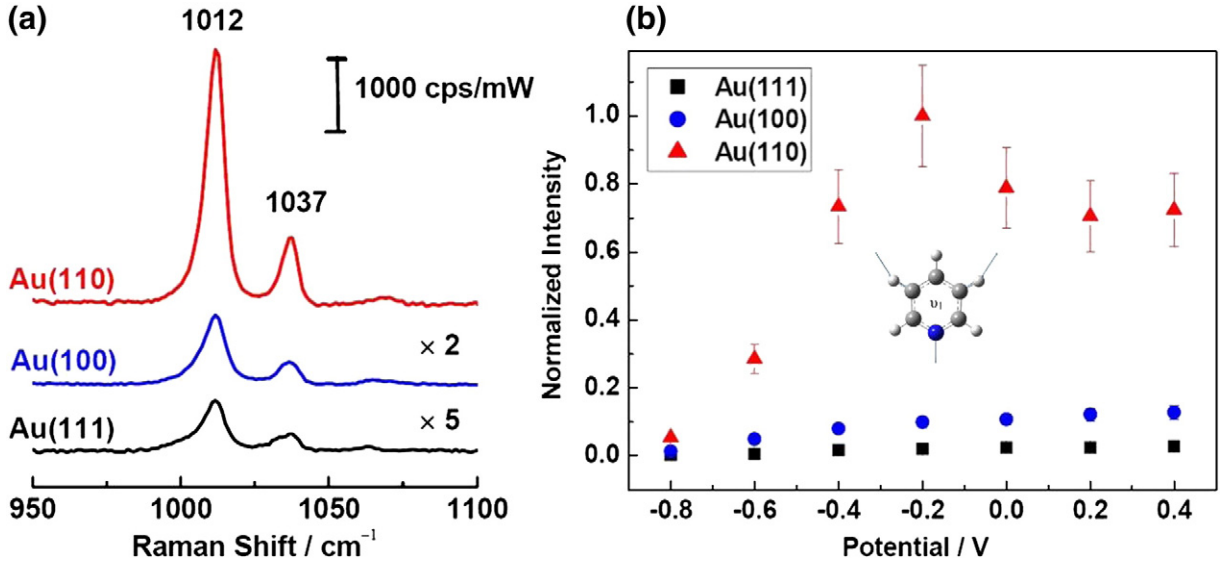

Fig. 10. (a) SHINER spectra of pyridine adsorbed on Au(111), Au(100) and Au(110) at 0.00 V. Electrolyte: 10 mM pyridine + 0.1 M $NaClO_4$. (b) Normalized SHINER intensities of the ring breathing mode υ_1 (the inset figure) for pyridine on Au(111), Au(100) and Au(110) at different potentials.
Reproduced by permission of American Chemical Society, from Li et al. [18].

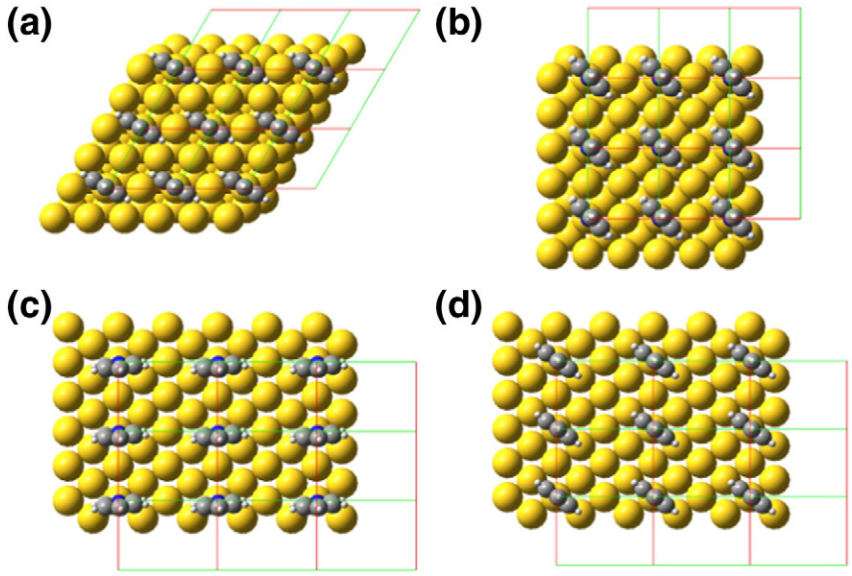

Fig. 11. The optimized geometry of pyridine on (a) Au(111), (b) Au(110)–[001], (c) Au(110)–[1$\bar{1}$0] and (d) Au(100).

Table 1
Calculated bond length of N – Au, N – C, the interaction energy between pyridine and the surfaces, *zz* component of the polarizability α_{zz} of the clean surface (S) and of the pyridine–surface (Py–S) complexes, and the Raman scattering factor S_1 of the ring breathing mode υ_1.

Py–Au(*hkl*)	B(N–Au)[a]	B(N–C)[a]	E_{int}	α_{zz} ($\times 10^4$)		S_1($\times 10^5$)[e]
−(2 × 2)			(Py–S)[b]	(S)[c]	(Py–S)[d]	
Au(111)	2.592	1.342	16.1	2.626	3.264	1.8
Au(100)	2.440	1.344	27.6	2.641	3.360	5.0
Au(110)[f]	2.328	1.345	42.3	2.827	3.661	5.2
Au(110)[g]	2.342	1.345	41.9	2.827	3.673	6.9

[a] Bond length in Å; [b] interaction energy in kJ mol^{-1}; [c, d] polarizability in Å^3 and [e] Raman scattering factor in Å^4/amu; [f] and [g] are the two Py-Au(110) (2 × 2) configuration with the pyridine plane site along [001] and [1$\bar{1}$0], respectively.

and may create several opportunities for the further expanding of the depth and breadth of the current interfacial electrochemistry.

Acknowledgments

This work was financially supported by NSF of China for innovative research on “interfacial electrochemistry” (20321062), Ministry of Science and Technology (2011YQ030124), and NCF of NOW for a grant of computer time on Huygens. We also thank Profs. Jun Cheng, Xiao-Yu Cao and Dr. Xue-Ming Zhang for the English editing of this manuscript.

Appendix A. Supplementary data

Supplementary data to this article can be found online at http://dx.doi.org/10.1016/j.susc.2014.07.019.

References

[1] A.J. Bard, L.R. Faulkner, Electrochemical methods: fundamentals and applications, Wiley, New York, 2001.
[2] S.-G. Sun, P.A. Christensen, A. Wieckowski, In-situ spectroscopic studies of adsorption at the electrode and electrocatalysis, Elsevier, New York, 2007.
[3] M.J. Weaver, X. Gao, Annu. Rev. Phys. Chem. 44 (1993) 459.
[4] Z.-Q. Tian, B. Ren, Annu. Rev. Phys. Chem. 55 (2004) 197.
[5] Y.-F. Huang, D.-Y. Wu, H.-P. Zhu, L.-B. Zhao, G.-K. Liu, B. Ren, Z.-Q. Tian, Phys. Chem. Chem. Phys. 14 (2012) 8485.
[6] M. Fleischmann, P.J. Hendra, A.J. McQuillan, Chem. Phys. Lett. 26 (1974) 163.
[7] D.L. Jeanmaire, R.P. Van Duyne, J. Electroanal. Chem. 84 (1977) 1.
[8] M.G. Albrecht, J.A. Creighton, J. Am. Chem. Soc. 99 (1977) 5215.
[9] M. Moskovits, J. Chem. Phys. 69 (1978) 4159.
[10] J.A. Creighton, C.G. Blatchford, M.G. Albrecht, J. Chem. Soc. Faraday Trans. 2 (75) (1979) 790.
[11] S.-Y. Ding, X.-M. Zhang, B. Ren, Z.-Q. Tian, Surface-Enhanced Raman Spectroscopy (SERS): general introduction, Encyclopedia of Analytical ChemistryJohn Wiley & Sons, Ltd., 2014
[12] H. Wei, H. Xu, China Sci. B 40 (2010) 1.
[13] Z.-Q. Tian, B. Ren, J.-F. Li, Z.-L. Yang, Chem. Commun. (2007) 3514.
[14] V. Deckert, J. Raman Spectrosc. 40 (2009) 1336.
[15] Y.-X. Chen, A. Otto, J. Raman Spectrosc. 36 (2005) 736.
[16] A. Otto, Z. Phys. A Hadrons Nucl. 216 (1968) 398.
[17] J.-F. Li, Y.F. Huang, Y. Ding, Z.-L. Yang, S.B. Li, X.-S. Zhou, F.-R. Fan, W. Zhang, Z.-Y. Zhou, D.-Y. Wu, B. Ren, Z.L. Wang, Z.-Q. Tian, Nature 464 (2010) 392.
[18] J.-F. Li, S.-Y. Ding, Z.-L. Yang, M.-L. Bai, J.R. Anema, X. Wang, A. Wang, D.-Y. Wu, B. Ren, S.-M. Hou, T. Wandlowski, Z.-Q. Tian, J. Am. Chem. Soc. 133 (2011) 15922.
[19] J.-F. Li, A. Rudnev, Y. Fu, N. Bodappa, T. Wandlowski, ACS Nano 7 (2013) 8940.
[20] D.P. Butcher, S.P. Boulos, C.J. Murphy, R.C. Ambrosio, A.A. Gewirth, J. Phys. Chem. C 116 (2012) 5128.
[21] J.R. Anema, J.-F. Li, Z.-L. Yang, B. Ren, Z.-Q. Tian, Annu. Rev. Anal. Chem. 4 (2011) 129.
[22] N.R. Honesty, A.A. Gewirth, J. Raman Spectrosc. 43 (2012) 46.
[23] V. Uzayisenga, X.-D. Lin, L.-M. Li, J.R. Anema, Z.-L. Yang, Y.-F. Huang, H.-X. Lin, S.-B. Li, J.-F. Li, Z.-Q. Tian, Langmuir 28 (2012) 9140.
[24] X.-D. Tian, B.-J. Liu, J.-F. Li, Z.-L. Yang, B. Ren, Z.-Q. Tian, J. Raman Spectrosc. 44 (2013) 994.
[25] S.-B. Li, L.-M. Li, R. Anema Jason, B. Ren, J.-J. Sun, Z.-Q. Tian, Z. Phys. Chem. Int. J. Res. Phys. Chem. Chem. Phys. 225 (2011) 775.
[26] B.-Q. Zhang, S.-B. Li, Q. Xiao, J. Li, J.-J. Sun, J. Raman Spectrosc. 44 (2013) 1120.
[27] J.F. Li, X.D. Tian, S.B. Li, J.R. Anema, Z.L. Yang, Y. Ding, Y.F. Wu, Y.M. Zeng, Q.Z. Chen, B. Ren, Z.L. Wang, Z.Q. Tian, Nat. Protoc. 8 (2013) 52.
[28] X.-D. Lin, V. Uzayisenga, J.-F. Li, P.-P. Fang, D.-Y. Wu, B. Ren, Z.-Q. Tian, J. Raman Spectrosc. 43 (2012) 40.
[29] X.-D. Lin, J.-F. Li, Y.-F. Huang, X.-D. Tian, V. Uzayisenga, S.-B. Li, B. Ren, Z.-Q. Tian, J. Electroanal. Chem. 688 (2013) 5.
[30] M. Kerker, D.-S. Wang, H. Chew, Appl. Opt. 19 (1980) 4159.
[31] S. Chen, L. Meng, H. Shan, J. Li, Z. Yang, Z. Tian, Surface Plasmon Resonance modes and hot spots transfer based on SHINERS, 2014. (in preparation).
[32] G. Kresse, J. Furthmuller, Phys. Rev. B 54 (1996) 11169.
[33] J. Lipkowski, L. Stolberg, Adsorption of molecules at metal electrodes, in: J. Lipkowski, P.N. Ross (Eds.), Frontiers of electrochemistry, VCH, New York, Weinheim, 1992, p. 171.
[34] J.-F. Li, Z.-Q. Tian, Shell-Isolated Nanoparticle-Enhanced Raman Spectroscopy (SHINERS), in: Y. Ozaki, K. Kneipp, R. Aroca (Eds.), Frontiers of Surface-Enhanced Raman Scattering: Single Nanoparticles and Single Cells, Wiley, Singapore, 2014, p. 163.
[35] B. Gallinet, T. Siegfried, H. Sigg, P. Nordlander, O.J.F. Martin, Nano Lett. 13 (2012) 497.
[36] J. Ye, F. Wen, H. Sobhani, J.B. Lassiter, P.V. Dorpe, P. Nordlander, N.J. Halas, Nano Lett. 12 (2012) 1660.

[37] Y. Chu, D. Wang, W. Zhu, K.B. Crozier, Opt. Express 19 (2011) 14919.
[38] Y. Chu, W. Zhu, D. Wang, K.B. Crozier, Opt. Express 19 (2011) 20054.
[39] A. Ahmed, R. Gordon, Nano Lett. 12 (2012) 2625.
[40] L.A. Dick, A.D. McFarland, C.L. Haynes, R.P. Van Duyne, J. Phys. Chem. B 106 (2001) 853.
[41] A.R. Guerrero, R.F. Aroca, Angew. Chem. Int. Ed. Engl. 50 (2011) 665.
[42] J. Lipkowski, L. Stolberg, D.F. Yang, B. Pettinger, S. Mirwald, F. Henglein, D.M. Kolb, Electrochim. Acta 39 (1994) 1045.
[43] J. Lipkowski, L. Stolberg, S. Morin, D.E. Irish, P. Zelenay, M. Gamboa, A. Wieckowski, J. Electroanal. Chem. 355 (1993) 147.